Preprint submitted to Elsevier, Int. J. Hydrogen Energy, DOI: 10.1016/j.ijhydene.2016.05.211

Solar Thermochemical Hydrogen Production Using Ceria Zirconia Solid Solutions: Efficiency Analysis.

B. Bulfin,*[a] M. Lange[a], L. de Oliveira[a], M. Roeb[a], and C. Sattler[a]

In this work thermochemical hydrogen production using ceria zirconia redox materials of the form $Ce_{1-x}Zr_xO_2$, with x varied in the range 0 to 0.2, is investigated. A number of literature sources are used to fix the thermodynamic properties such as the partial molar entropies and enthalpies of reduction. From this, a full thermodynamic analysis of the fuel production is possible, where the heat required was assumed to be supplied by concentrated solar power. An efficiency model is presented and the materials are compared. The extent of reduction for a given temperature and oxygen partial pressure increases with increasing Zr concentration. However, the addition of Zr also has a negative effect on the oxidation reaction, requiring lower temperature oxidation and thus a larger temperature swing between the reaction steps. The thermodynamic analysis suggests that for cycles with a reduction temperature of 1773 K, the improvement in yield offered by $Ce_{1-x}Zr_xO_2$ does improve the efficiency, with $Ce_{0.8}Zr_{0.2}O_2$ having the highest solar to fuel production efficiency of the materials considered. To achieve this efficiency the oxidation would need to be performed at lower temperature (≤ 800 °C for $Ce_{0.8}Zr_{0.2}O_2$) than is common in experimental demonstrations, and may be kinetically limited.

Thermochemcial cycles driven by concentrated solar power have been heavily investigated as a method of renewable hydrogen production[1–6]. An example of such a cycle is illustrated in figure 1, which shows a schematic of a two-step metal oxide redox cycle, where the oxide is reduced at high temperature releasing oxygen and then the reduced oxide is re-oxidised with steam producing hydrogen.

This work is focused on two-step thermochemical cycles utilizing ceria based materials as the redox pair. Ceria can be partially reduced at high temperatures[7,8], with very rapid kinetics[9,10], and while remaining in the fluorite phase[11–13]. The fact that there is no phase change means that ceria reduction and oxidation offers a very practical and achievable thermochemical cycle for fuel production[14]. The reduced ceria can then be used to split both H_2O and CO_2, producing hydrogen and carbon monoxide respectivly[15]. This process has been extensively investigated in recent years both theoretically[16–21] and experimentally[22–24]. Recently, Marxer *et al.* used cerium dioxide to perform over 200 cycles in a lab scaled reactor, producing 700 standard litres of syn-gas, which was then processed via the Fischer-Tropsch process to produce Kerosene[25].

The redox properties of CeO_2 can be somewhat tuned by replacing some of the cerium cations in the fluorite crystal structure with other metals. The addition of ions which have the same valence, but lower ionic radius than ceria, such as Zr^{4+} and Hf^{4+}, can increase the reducibility[26–34]. This is very important as the reduction is the energy intensive step, suggesting there could be benefits for the overall efficiency of the cycles[35].

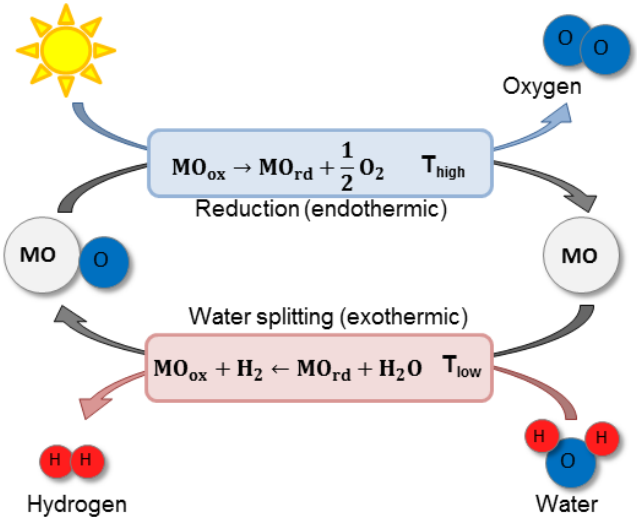

Fig. 1 A schematic showing a two-step thermochemical hydrogen production cycle using a metal oxide as the redox material and powered by solar energy.

Preprint submitted to International Journal of Hydrogen Energy , DOI: http://dx.doi.org/10.1016/j.ijhydene.2016.05.211

[a] *Institute of Solar Research, German Aerospace Center, 51147 Cologne. Tel: +49 (0)2203 6014130; E-mail: bulfinb@tcd.ie*

A recent study by Takacs *et al.* suggests that although Zr improves the reducibility of ceria, it also negatively impacts the water splitting step, and ultimately offers no improvement in hydrogen production efficiency[36]. However, in this study the yield was fixed and the reduction temperature was set accordingly. This could nullify the positive effect Zr has on the yield. Here we expand upon this work, investigating more Zr concentrations and use a more sophisticated efficiency model with a more in-depth look at the oxidation step.

Thermodynamic data from the literature for both CeO_2 [7,37–39] and $Ce_{1-x}Zr_xO_2$ [35,36,40] is used to perform a fully optimised thermodynamic analysis of solar hydrogen production. Higher concentrations of Zr ($x > 0.2$) could not be considered in this work due to a lack of thermodynamic data in the literature.

1 Thermodynamics

In order to perform an efficiency analysis, one must first know the thermodynamic properties of the reactions. The cerium dioxide thermochemical water splitting cycle is described by

$$CeO_{2-\delta_{ox}} \xrightarrow{heat = \Delta h^\circ_{rd}} CeO_{2-\delta_{rd}} + \frac{\Delta\delta}{2} O_2 \qquad T_{rd}, \quad (1)$$

$$CeO_{2-\delta_{rd}} + \Delta\delta\, H_2O \longrightarrow CeO_{2-\delta_{ox}} + \Delta\delta H_2 \qquad T_{ox}, \quad (2)$$

$$\Delta T = T_{rd} - T_{ox} \quad \text{and} \quad \Delta\delta = \delta_{rd} - \delta_{ox}, \quad (3)$$

where the the reactions in equation 1 and 2 sum to water splitting. The ceria is reduced at a temperature T_{rd}, to a vacancy concentration of δ_{rd}. It is oxidised at a temperature T_{ox} in a 1 bar H_2O atmosphere to a vacancy concentration δ_{ox}. The maximum yield per cycle and per mole of metal oxide is the difference in the equilibrium vacancy stoichiometry $\Delta\delta$. For convenience, the deviations from stoichiometry δ, is defined as a unit-less oxygen vacancy concentration

$$\delta = \frac{[O_{vac}]}{[Ce]}, \quad (4)$$

where $[O_{vac}]$ is the concentration of oxygen vacancies and $[Ce]$ is the concentration of cerium atoms.

Since 1 and 2 sum to water splitting, their change in Gibbs free energies must also sum to that of the water splitting reaction, namely

$$\Delta g^\circ_{O,ws} = \Delta g^\circ_{O,rd} + \Delta g^\circ_{O,ox}, \quad (5)$$

where the subscript O indicates per mole of atomic oxygen. Given that $\Delta g^\circ_{O,ws}$ is known, an expression for $\Delta g^\circ_{O,rd}$ will also give the thermodynamics of the oxidation reaction.

The standard partial molar change in Gibbs free energy for the reduction reaction is given by

$$\Delta g^\circ_{O,rd}(\delta, T) = \Delta h^\circ_{O,rd}(\delta) - T\Delta s^\circ_{O,rd}(\delta), \quad (6)$$

where $\Delta h^\circ_{O,rd}$ and $\Delta s^\circ_{O,rd}$ are the standard partial molar enthalpy and entropy of the reduction reaction given in equation 1. Partial molar enthalpy and entropy values from the literature were fit empirically, with the fits shown in figure 2 and 3. This shows the effect that adding Zr to ceria has on the redox thermodynamics. It reduces the change in enthalpy of the reduction reaction, which should allow the material to be more easily reduced. However, it also reduces the change in entropy, which according to equation 6 also reduces the the driving force $T\Delta s^\circ_{O,rd}$, for the reduction reaction.

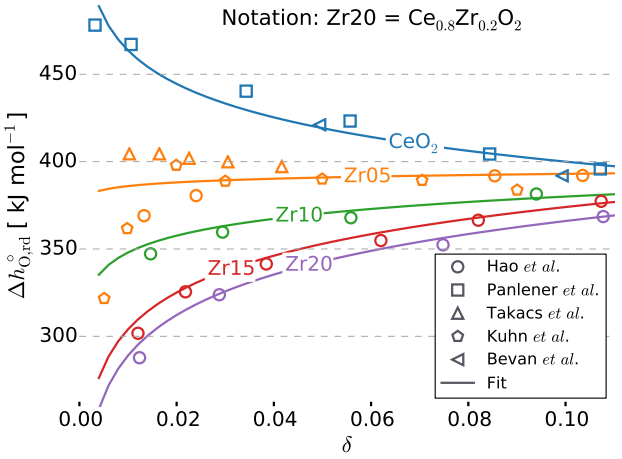

Fig. 2 $\Delta h^\circ_{O,rd}(\delta)$ fits of CeO_2 [7,37–39], $Ce_{0.95}Zr_{0.05}O_2$ [35,36,40] and $Ce_{1-x}Zr_xO_2$ for x =0.1, 0.15, 0.2 [35], are plotted along with some of the literature data.

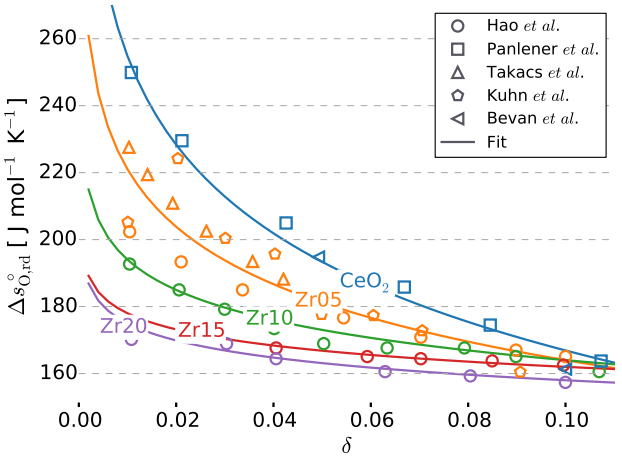

Fig. 3 $\Delta s^\circ_{O,rd}(\delta)$ fits for CeO_2 [7,37–39], $Ce_{0.95}Zr_{0.05}O_2$ [35,36,40] and $Ce_{1-x}Zr_xO_2$ for x =0.1, 0.15, 0.2 [35], are plotted along with some of the literature data.

An equation of state for the reduction reaction can be obtained using the formulae

$$\Delta g_{O,rd}(\delta, T) = \Delta g^\circ_{O,rd} + \frac{1}{2} RT \ln\left(\frac{p_{O_2}}{p^\circ}\right), \quad (7)$$

which at equilibrium must be zero, and so using equation 6 and the fit values of entropy and enthalpy gives the relation

$$\Delta h^\circ_{O,rd}(\delta) - T\Delta s^\circ_{O,rd}(\delta) = -\frac{1}{2} RT \ln\left(\frac{p_{O_2}}{p^\circ}\right). \quad (8)$$

This equation gives a relation between δ, T, and p_{O_2}, which can be solved to obtain $\delta_{rd}(T, p_{O_2})$, or indeed the equilibrium partial

pressure $p_{O_2}(\delta,T)$. It also allows $\delta_{ox}(T)$ to be determined, by setting the oxygen partial pressure equal to the value one would have in steam at the same temperature [18].

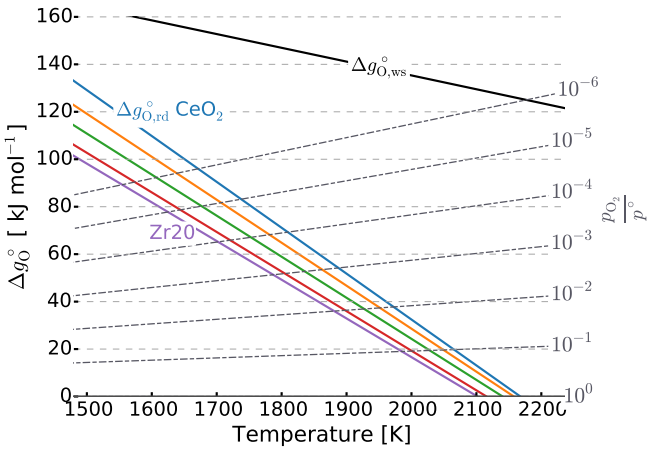

Fig. 4 $\Delta g^\circ_{O,rd}$ vs. T for $\delta = 0.05$ (and for reference $\Delta g^\circ_{O,ws}$). Also plotted are the lines of pumping work $\frac{1}{2}RT\ln\left(\frac{p_{O_2}}{p^\circ}\right)$, for a range of partial pressures labelled on the right axis.

The thermodynamic condition given in equation 7 can be visualised with an Ellingham diagram, as seen in figure 4. This is a plot of the Gibbs free energy of a reaction versus temperature, which can be obtained using equations 5 and 6 from the values shown in figures 2 amd 3. In order for a reaction to proceed spontaneously it must have a negative change in Gibbs free energy, $\Delta g < 0$. Figure 4 shows that the addition of Zr reduces $\Delta g^\circ_{O,rd}$, with larger concentrations of Zr having a stronger effect. This is in line with the fact that the addition of Zr makes ceria easier to reduce.

The Gibbs free energy of reduction can also be decreased by reducing the oxygen partial pressure as seen in equation 7. The reduction temperature for a given oxygen partial pressure is the intercept between the $\Delta g^\circ_{O,rd}$ line, and the partial pressure lines (pumping work), which is where $\Delta g_{O,rd} = 0$.

Next we must determine the thermodynamic limitations of the oxidation reaction. For a given hydrogen steam ratio the oxidation reaction obeys the condition

$$\Delta g_{O,ox}(\delta,T) = \Delta g^\circ_{O,ox} + RT\ln\left(\frac{p_{H_2}}{p_{H_2O}}\right), \tag{9}$$

which at equilibrium is equal to zero. In this case $\Delta g^\circ_{O,ox}(\delta,T)$, can be calculated using equations 5 and 6, and the known values of $\Delta g^\circ_{O,ws}$.

An Ellingham diagram for the oxidation reaction is plotted in figure 5, which shows the condition given in equation 9. We see that in order for the oxidation reaction to proceed spontaneously ($\Delta g < 0$), requires relatively low temperatures when compared to the reduction reaction. For lower hydrogen to steam ratios the reaction proceeds at higher temperatures, indicated by the intercept between the $\Delta g^\circ_{O,ox}$ lines and the the dashed lines for different hydrogen partial pressures.

In figure 5 the oxidation temperature can be seen to decreases

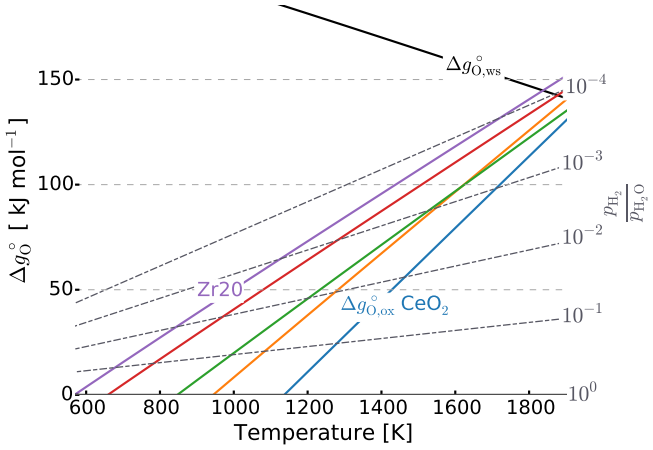

Fig. 5 $\Delta g_{O,ox}$ vs. T for $\delta = 0.02$. Also plotted are lines of $RT\ln\left(\frac{p_{H_2}}{p_{H_2O}}\right)$, with the pressure ratio indicated on the right axis.

with increasing Zr content. This illustrates the fact that although Zr improves the reducibility of ceria, it also has a negative impact on the water splitting thermodynamics. From figures 4 and 5, one would expect that for $Ce_{1-x}Zr_xO_2$ thermochemical cycles, the temperature swing ΔT, would increase with the concentration of Zr. It remains to be seen if indeed this large temperature swing will also result in a lower efficiency due to more energy being required to heat the oxide.

2 Efficiency Model

The efficiency model used here is based on that used in a previous publication by the authors [18], and is also very similar to a more general efficiency optimisation performed recently by Jarrett *et al.* [41]. The solar to fuel efficiency is given by the equation

$$\eta_{fuel} = \frac{\eta_{plant}\,\alpha\,\Delta\delta\,\mathrm{HHV}_{H_2}}{Q_{total}}, \tag{10}$$

where , $\alpha\,\Delta\delta\,\mathrm{HHV}_{H_2}$ is the energy stored in the fuel, Q_{total} is the total energy required for the process and η_{plant} is the efficiency at which the solar energy is supplied by the concentrated solar plant. Here, α is reacted fraction for the oxidation reaction, as stopping the oxidation reaction before completion can improve the efficiency [14,15]. The plant efficiency can be defined as

$$\eta_{plant}(T_{rd},C) = \frac{(0.65C \times 1\,\mathrm{kW\,m^{-2}} - \sigma(T_{rd}^4 - T_{amb}^4))}{C \times 1\,\mathrm{kW m^{-2}}}, \tag{11}$$

where the solar irradiance is set at 1 $\mathrm{kW\,m^{-2}}$, the ratio of the reflector area to the recievier is taken as $C = 3000$, the factor of 0.65 is the annual average optical efficiency of the solar collection system [42,43], and the $\sigma(T_{rd}^4 - T_{amb}^4)$ accounts for re-radiation.

The total energy required for the cycle is given by

$$Q_{total} = Q_{rd} + Q_{CeO_2} + Q_{pmp} + Q_{H_2O} - Q_{rec}, \tag{12}$$

which is the energy required to reduce the ceria Q_{rd}, heat the ceria Q_{CeO_2}, reduce the pressure Q_{pmp}, heating steam for the oxidation Q_{H_2O} and finally the heat which may be recycled from

the oxidation step of the reaction and from cooling the ceria Q_{rec}. A schematic giving an overview of the process and showing the various heat requirements can be seen in figure 6.

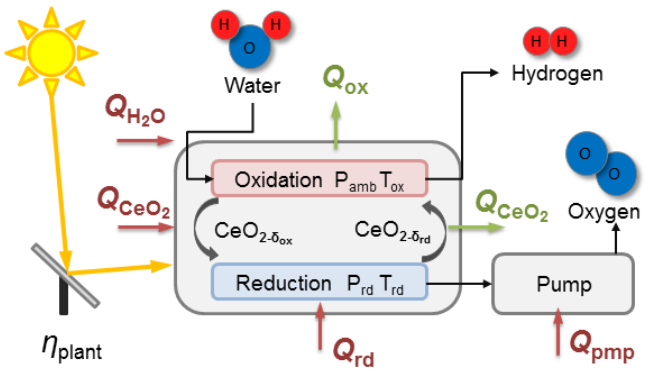

Fig. 6 Schematic of the process showing the various heat inputs and outputs.

Although there have been a number of methods proposed for exchanging heat between hot and cold ceria [44–46], they are rather complicated and have not been shown to operate effectively in practice. Instead here the recycled heat in this case was assumed to be used for the lower temperature energy requirements - heating the steam or being converted to electricity to power the vacuum pumps. Sweep gas was not considered as a means of reducing the partial pressure, as previous work by Bulfin *et al.* [18] and Brendelberger *et al.* [47] have suggested that vacuum operation can offer better efficiency.

2.1 Heat costs

Here we give a break down of how each heat requirement term is calculated. It should be noted that all terms are per mole of ceria cycled.

Full re-oxiation of the ceria to δ_{ox} does not in general offer optimal efficiency, and so it is useful to introduce a stopping point for the oxidation reaction,

$$\delta_{\mathrm{ox}}(\alpha) = \delta_{\mathrm{ox}} + (1-\alpha)\Delta\delta, \quad 0 < \alpha \leq 1, \tag{13}$$

where α is the completed fraction of the oxidation reaction. Setting α to values less than one stops the oxidation reaction short of equilibrium. The energy required to reduce a mole of ceria is then

$$Q_{\mathrm{rd}} = \int_{\delta_{\mathrm{ox}}(\alpha)}^{\delta_{\mathrm{rd}}} \Delta h^{\circ}_{\mathrm{O,rd}}(\delta)\, d\delta \quad [\mathrm{J\,mol^{-1}}].$$

The energy cost of heating the ceria is given by

$$Q_{\mathrm{CeO_2}} = \int_{T_{\mathrm{ox}}}^{T_{\mathrm{rd}}} C_{p_{\mathrm{CeO_2}}}(T)\, dT \quad [\mathrm{J\,mol^{-1}}], \tag{14}$$

where the molar specific heat capacity of ceria was obtained from the work of Pankratz [48], and fit with a polynomial. Given that $Ce_{1-x}Zr_xO_2$ has the same crystal structure as ceria, all materials were assumed to have the same molar specific heat capacity.

The energy required to pump the system during reduction is Q_{pmp}. It makes sense to only pump once the reactor has reached T_{rd}, as this maximises the equilibrium oxygen partial pressure $p_{\mathrm{O_2}}(\delta, T)$, and thus reduces the amount of pumping work necessary. Here we consider the optimal case, where oxygen is pumped off at its equilibrium pressure [49], thus minimizing the work. The upper pressure is restricted to a maximum of ambient pressure giving a pumping pressure of

$$p_{\mathrm{pmp}}(\delta, T) = \begin{cases} p_{\mathrm{amb}} & : p_{\mathrm{O_2}}(\delta, T) > p_{\mathrm{amb}} \\ p_{\mathrm{O_2}}(\delta, T) & : p_{\mathrm{amb}} > p_{\mathrm{O_2}}(\delta, T) \end{cases} \tag{15}$$

The energy required to pump per mole of vacancies is then assumed to be that of pumping an ideal gas

$$\frac{\partial Q_{\mathrm{pmp}}}{\partial \delta} = \frac{1}{2}\frac{RT}{\eta_{\mathrm{pmp}}(p_{\mathrm{pmp}})} \ln\left(\frac{p_{\mathrm{pmp}}(\delta, T_{\mathrm{rd}})}{p_{\mathrm{amb}}}\right), \tag{16}$$

where the pumping efficiency decreases with pressure and is given by the same power law as in previous work by the authors [18].

$$\eta_{\mathrm{pmp}}(P) = 0.4\, P^{0.544}, \tag{17}$$

where the factor of 0.4 is to account for heat being converted to electricity to power the pumps. The total energy required for pumping is then

$$Q_{\mathrm{pmp}} = \int_{\delta_{\mathrm{ox}}(\alpha)}^{\delta_{\mathrm{rd}}} \frac{\partial Q_{\mathrm{pmp}}}{\partial \delta}\, d\delta. \tag{18}$$

The steam for oxidation must be heated to the oxidation temperature. A heat exchanger can be used to heat the oxidiser using the out flowing oxidiser and fuel. The energy required for oxidation is then given by

$$Q_{\mathrm{H_2O}} = n_{\mathrm{H_2O}}(1-\varepsilon_{\mathrm{gas}})\left(\int_{100}^{T_{\mathrm{ox}}} C_{p_{\mathrm{H_2O}}}(T)dT + L_{\mathrm{H_2O}}\right), \tag{19}$$

where $L_{\mathrm{H_2O}}$ is the latent heat of vaporization of water, the heat exchange effectiveness was set to $\varepsilon_{\mathrm{gas}} = 0.85$ in all cases and $n_{\mathrm{H_2O}}$ is calculated from equilibrium considerations (see next section).

Heat can be recovered from the hot ceria as it cools and there is also heat released during oxidation

$$Q_{\mathrm{ox}} = Q_{\mathrm{rd}} - \alpha\,\Delta\delta\,\mathrm{LHV}_{\mathrm{H_2}}. \tag{20}$$

The amount of recovered heat is limited by the total heat required for the lower temperature processes giving the conditions

$$\begin{aligned} Q_{\mathrm{rec}} &= \varepsilon_{\mathrm{rec}}(Q_{\mathrm{ox}} + Q_{\mathrm{CeO_2}}), \\ Q_{\mathrm{rec}} &\leq Q_{\mathrm{pmp}} + Q_{\mathrm{H_2O}}. \end{aligned} \tag{21}$$

Note that it is assumed that the hot ceria from the reduction step is not used to heat the relatively cooler ceria coming from the oxidation step as such a heat exchanger would be extremely difficult to realise. Using this heat however for lower temperature process heat requirements should be more feasible. The heat exchange effectiveness $\varepsilon_{\mathrm{rec}}$ was set to 0.9 for all calculations.

2.2 Number of moles of steam $\mathbf{n}_{H_2O}$

Setting equation 9 for the oxidation reaction equal to zero gives the equilibrium condition

$$\Delta g^{\circ}_{O,ox}(T) = -RT \ln\left(\frac{p_{H_2}}{p_{H_2O}}\right), \tag{22}$$

which can be re-arranged to give the equilibrium ratio between H_2 and H_2O as

$$R_{\frac{H_2}{H_2O}}(\delta,T) = \frac{p_{H_2}}{p_{H_2O}} = \exp\left(\frac{-\Delta g^{\circ}_{ox}(T)}{RT}\right). \tag{23}$$

The equilibrium mole fraction of H_2 is then

$$\frac{x_{H_2}}{1} = \frac{\frac{x_{H_2}}{x_{H_2O}}}{\frac{x_{H_2O}}{x_{H_2O}} + \frac{x_{H_2}}{x_{H_2O}} + \frac{x_{O_2}}{x_{H_2O}}} \approx \frac{R_{\frac{H_2}{H_2O}}}{1 + R_{\frac{H_2}{H_2O}}}, \tag{24}$$

since $x_{H_2O} + x_{H_2} + x_{O_2} = 1$ and $x_{O_2} << x_{H_2O} + x_{H_2}$ as free oxygen is consumed by the ceria. To get the mole fraction of hydrogen produced by the reaction with ceria, the equilibrium hydrogen in a pure steam atmosphere must also be subtracted giving

$$x_{H_2}(\delta,T) = \frac{R_{\frac{H_2}{H_2O}}(\delta,T)}{1 + R_{\frac{H_2}{H_2O}}(\delta,T)} - x_{H_2}(T)_{eq}, \tag{25}$$

where $x_{H_2}(T_{ox})_{eq}$ is the equilibrium mole fraction of hydrogen in an isolated H_2O atmosphere at temperature T_{ox}.

The minimum number of moles of oxidiser required per mole of vacancies is then

$$\frac{\partial n_{H_2O}(\delta,T_{ox})}{\partial \delta} = \frac{1}{x_{H_2}(\delta,T_{ox})}, \tag{26}$$

with the total number of moles of oxidiser required to cycle one mole of ceria given by

$$n_{H_2O} = \int_{\delta_{ox}(\alpha)}^{\delta_{rd}} \frac{\partial n_{H_2O}(\delta,T_{ox})}{\partial \delta}\, d\delta. \tag{27}$$

Figure 7 shows the amount of steam required per mole of H_2 during the oxidation cycle. This highlights the cost that comes with adding Zr to ceria which increase the yield, but also significantly increases the amount of steam required for oxidation.

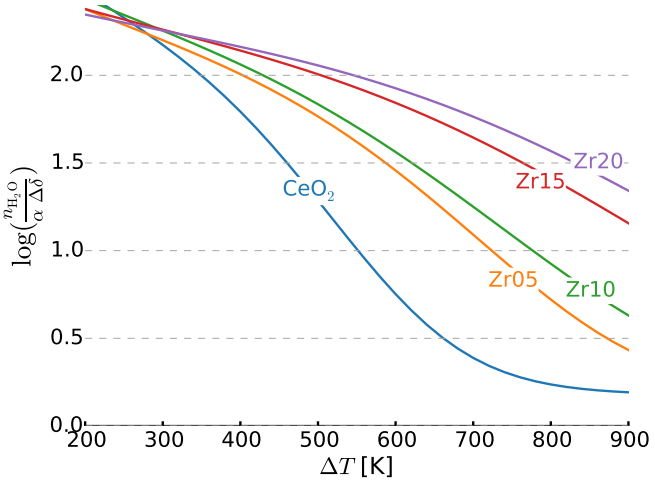

Fig. 7 The number of moles of steam which are required per mole of hydrogen produced $\log(\frac{n_{H_2O}}{\alpha\,\Delta\delta})$ vs. ΔT. Here $T_{rd} = 1773\,K$, $p_{O_2} = 5\times10^{-4}\,bar$ and $\alpha = 0.96$ for CeO_2 and 0.92 for the Zr added samples (see figure 9). The values of δ_{rd} in order from CeO_2-Zr20 were 0.03, 0.037, 0.041, 0.049 and 0.053.

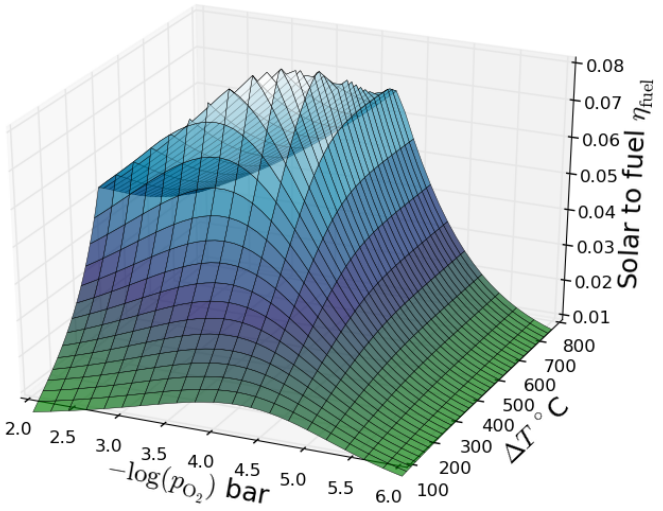

Fig. 8 A plot of fuel production efficiency for pure CeO_2 vs. ΔT and p_{O_2}. Here $T_{rd} = 1773K$ and the fraction complete $\alpha = 0.96$.

3 Results

For a given reduction temperature the efficiency can be optimised with respect to the temperature swing ΔT, the lower pressure at the end of reduction p_{O_2} and the fraction complete of the oxidation reaction α.

Figure 8 shows how the efficiency can be optimised with respect to ΔT and the oxygen partial pressure at the end of reduction p_{O_2}. The optimal ΔT arises because Q_{CeO_2} increases with the temperature swing, but the yield also increases and the amount of steam to be heated Q_{H_2O} decreases. There has been some research into performing the cycle isothermally, $\Delta T = 0$[50–53], which has also been demonstrated at the laboratory scale by Venstrom *et al.*[54]. However, the poor yield and large amount of pumping work required for isothermal cycles results in a very low efficiency[17,55].

The optimal p_{O_2} seen in figure 8 is due to the compromise between reducing the partial pressure to improve the yield, and the pumping efficiency decreasing with pressure (see equation 17). The sharp peak arises from the condition $Q_{rec} \leq Q_{pmp} + Q_{H_2O}$, which only allows recycled heat to be used for the lower temperature heat requirements.

Note that α is a very important parameter, especially in the case of the Zr added samples, as stopping the oxidation reaction short of complete re-oxidation can save a lot of energy by reducing the amount of steam required for oxidation. Figure 10 shows the effect α has on the solar to fuel efficiency. Here we see that the Zr added materials have an optimum efficiency at $\alpha \approx 0.92$, where as ceria has an optimal efficiency for $\alpha \approx 0.96$. For $\alpha > 0.97$ ceria performs better under all conditions, which is the same re-

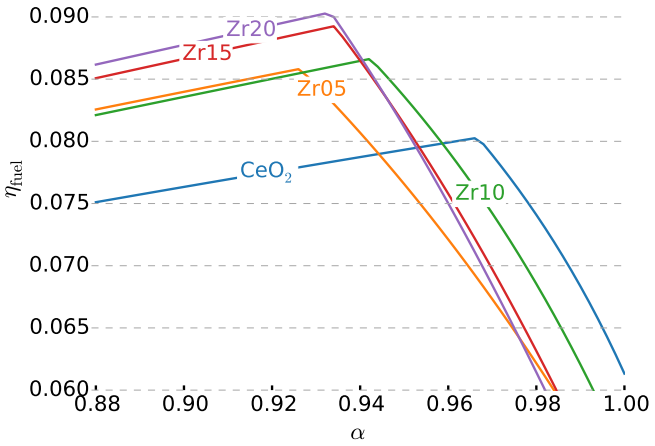

Fig. 9 Solar to fuel efficiency for the different materials vs. α, with heat recovery. The partial pressure at the end of reduction was set to $p_{O_2} = 5 \times 10^{-4}$ bar, $T_{rd} = 1773\,K$ and the optimal ΔT values from figure 11 were used.

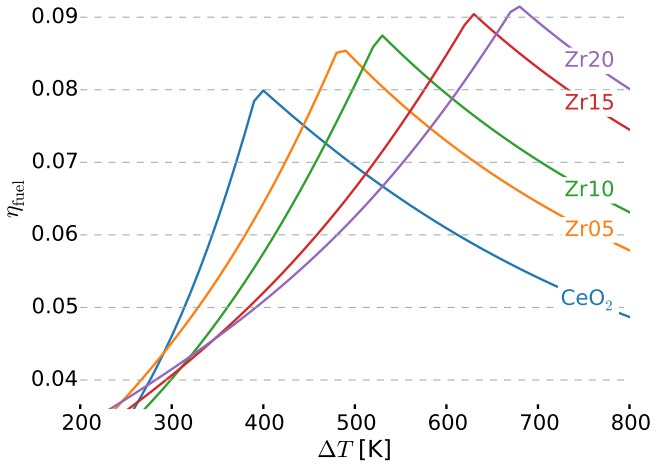

Fig. 11 Solar to fuel efficiency for the different materials vs. ΔT, with heat recovery from the ceria. The partial pressure at the end of reduction was set to $p_{O_2} = 5 \times 10^{-4}$ bar and $\alpha = 0.96$ for CeO_2 and 0.92 for the Zr added samples.

sult Takacs *et al.* found in their efficiency calculations[36].

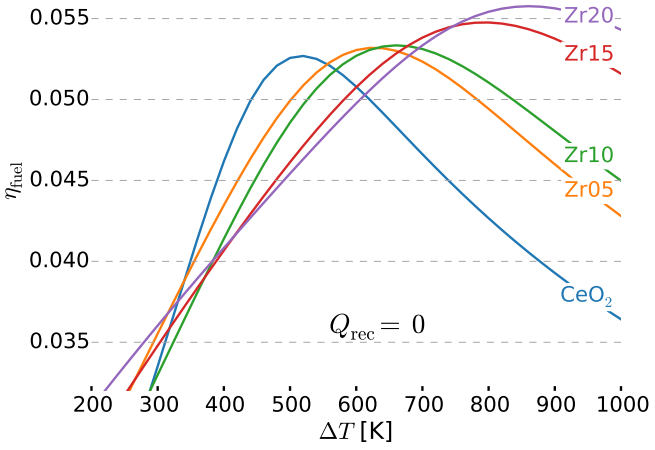

Fig. 10 Solar to fuel efficiency for the different materials vs. ΔT, without heat recovery. The partial pressure at the end of reduction was set to $p_{O_2} = 5 \times 10^{-4}$ bar and $\alpha = 0.96$ for CeO_2 and 0.92 for the Zr added samples.

Figure 10 shows the fuel production efficiency calculated for the different materials without heat recovery. There is no sharp peak in this case as there is no discontinuity condition on heat recycling. The optimal ΔT value increases for increasing Zr concentration which is in agreement with the data plotted in figure 4, namely that larger Zr concentrations require lower oxidation temperatures. Even so, the addition of Zr improves efficiency with Zr20 increasing the optimal efficiency by a factor of approximately 1.06 relative to that of ceria.

Figure 11 shows the fuel production efficiency with heat recovery, and again the peak efficiency increases further with increasing Zr concentration. This is because heat used to cycle the ceria is now used for lower temperature processes and increasing ΔT has a lower impact on the efficiency. Again here the highest efficiency was seen for Zr20 which at the optimal conditions was a factor of 1.12 times higher than for pure ceria. These results differ from those previously reported[36], which was likely due to the different efficiency calculation approaches and the inclusion here of a stopping point for the oxidation reaction, α.

Although Zr20 showed the best efficiency, there is the issue that performing oxidation at lower temperatures could be limited by kinetics. It was recently shown that increasing the Zr concentration in ceria also decreased the oxidation kinetics in pure oxygen[9,10]. It is therefore likely that in practice selecting the optimal Zr concentration will be a compromise between both thermodynamic and kinetic considerations.

3.1 Efficiency Outlook

The low efficiencies seen here are a result of the relatively modest model assumptions. Experimentally reported efficiency values do not include the losses due to solar collection. In this case the solar flux entering the reactor is $\approx 1950\,\text{kW}\,\text{m}^{-2}$, and the conversion of this energy to fuel is approximately 16 % for CeO_2 and 18.4 % for Zr20. The relative heat costs at optimal conditions for Zr20 and CeO_2 are shown in figure 12, with and without heat recovery. For all cases the energy required to heat the oxide is the largest heat cost, followed by re-radiation losses.

More generally an upper bound for the conversion efficiency of heat to fuel is given by $\frac{\text{HHV}_{H_2}}{\Delta H_{rd}}$, which for pure ceria is approximately 67 %, and for Zr20 it is 83 %. If some additional work is required then the heat to fuel conversion efficiency is limited by

$$\eta_{max} = \frac{\text{HHV}_{H_2}}{\Delta H_{rd} + \eta_w \Delta G_w}, \tag{28}$$

where ΔG_w is the additional work (pumping or sweep gas), and η_w is the efficiency at which this extra energy is supplied. This up-

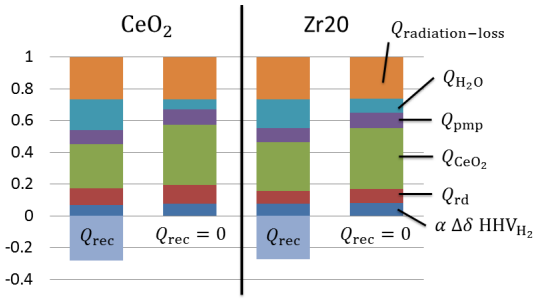

Fig. 12 The relative heat consumptions calculated using the formulae $\frac{Q}{Q_{\text{total}}+Q_{\text{rec}}+Q_{\text{radiation-loss}}}$ for both CeO_2 and Zr20, at the optimal efficiency conditions seen in both figure 10 ($Q_{\text{rec}} = 0$) and figure 11.

per limit would be achieved with 100 % efficient heat exchangers and if $\eta_w \Delta G_w$ is powered using recycled heat. If $\eta_w \Delta G_w$ is less than the available heat from the ceria, then high temperature ceria to ceria heat exchangers would be needed to reach this efficiency. In theory ΔG_w is relatively small, at around $50 kJ mol^{-1}$ to reduce the oxygen partial pressure to 10^{-4} bar. In this case with $\eta_w = 0.4$, the maximum efficiency for CeO_2 and Zr20 would be $\eta_{\max} \approx 50$ % and 65 % respectively. However, the efficiency η_w is generally very low and needs to be improved. This could be achieved by either improving pumping methods or sweep gas renewal technologies, and remains a challenge for the success of this technology.

4 Conclusions

The solar hydrogen production efficiency of a two-step thermochemical cycle using redox materials of the form $Ce_{1-x}Zr_xO_2$, with x varied in the range 0 to 0.2, was calculated and optimised with respect to the operating conditions. The efficiency analysis was relatively modest in terms of heat recovery, pumping work efficiency, and solar collection efficiency, resulting in low overall solar to fuel conversion efficiencies, with a maximum value calculated to be 9.5 %. It was however sufficient to compare the materials with the efficiency having a clear dependence on the Zr concentration. The addition of Zr to ceria improves the yield and the efficiency although it also requires oxidation to be performed at lower temperatures. For $Ce_{0.8}Zr_{0.2}O_2$ the optimal oxidation temperature found here was around 800 °C which could still be high enough that the oxidation reaction is not kinetically limited. Overall, the results suggest that an efficiency improvement can be achieved using materials of the form $Ce_{1-x}Zr_xO_2$, but in practice a compromise between thermodynamics and kinetics would be required to select the optimal Zr content.

Acknowledgements

This work has received funding from the Helmholtz Association VH-VI-509. Lukas Hoffmann provided assistance in producing the schematics.

Nomenclature

δ Oxygen stoichiometry in $CeO_{2-\delta}$

a° a at standard pressure

$\Delta g_{O,ws}$ Partial molar Gibbs energy for water splitting

$\Delta g_{O,rd}$ Partial molar Gibbs energy for reduction

$\Delta g_{O,ox}$ Partial molar Gibbs energy for oxidation

$\Delta h_{O,rd}$ Partial molar enthalpy of reduction

$\Delta s_{O,rd}$ Partial molar entropy of reduction

T_{rd} Reduction temperature

T_{ox} Oxidation temperature

T_{amb} Ambient temperature

ΔT $T_{rd} - T_{ox}$

δ_{rd} Reduced stoichiometry

δ_{ox} Maximum oxidised stoichiometry

$\Delta\delta$ Maximum yield $\delta_{rd} - \delta_{ox}$

p_{O_2} Oxygen partial pressure

HHV_{H_2} Higher heating value of hydrogen

p° Standard pressure

Q_{rd} Energy consumed by reduction

Q_{CeO_2} Energy used to heat ceria

Q_{pmp} Energy required to pump oxygen

Q_{H_2O} Energy required to heat oxidiser

Q_{ox} Energy released by oxidation reaction

Q_{rec} Recovered process heat

C_p Specific heat capcity

ε Heat exchanger effectiveness

n_i Moles of component i

η_i Efficiency of process i

C Solar concentration

L_{H_2O} Latent heat of vaporization

References

References

1 T. Kodama, *Prog. Energy Combust. Sci.*, 2003, **29**, 567–597.

2 A. Steinfeld, P. Kuhn, A. Reller, R. Palumbo, J. Murray and Y. Tamaura, *Int. J. Hydrogen Energy*, 1998, **23**, 767–774.

3 S. Abanades, P. Charvin, G. Flamant and P. Neveu, *Energy*, 2006, **31**, 2805–2822.

4 M. Roeb, M. Neises, N. Monnerie, F. Call, H. Simon, C. Sattler, M. Schmücker and R. Pitz-Paal, *Materials*, 2012, **5**, 2015–2054.

5 C. Perkins and A. W. Weimer, *Int. J. Hydrogen Energy*, 2004, **29**, 1587–1599.

6 M. Roeb, M. Neises, J.-P. Säck, P. Rietbrock, N. Monnerie, J. Dersch, M. Schmitz and C. Sattler, *Int. J. Hydrogen Energy*, 2009, **34**, 4537–4545.

7 R. Panlener, R. Blumenthal and J. Garnier, *J. Phys. Chem. Solids*, 1975, **36**, 1213–1222.

8 S. Abanades and G. Flamant, *Sol. Energy*, 2006, **80**, 1611–1623.

9 B. Bulfin, A. J. Lowe, K. A. Keogh, B. E. Murphy, O. Lubben, S. A. Krasnikov and I. V. Shvets, *J. Phys. Chem. C*, 2013, **117**, 24129–24137.

10 B. Bulfin, F. Call, J. Vieten, M. Roeb, C. Sattler and I. Shvets, *J. Phys. Chem. C*, 2016.

11 Y. Ban and A. S. Nowick, Proceeding of the 5th Materials research symposium, 1972, p. 353.

12 A. Bonk, A. Remhof, A. C. Maier, M. Trottmann, M. V. Schlupp, C. Battaglia and U. F. Vogt, *J. Phys. Chem. C*, 2015.

13 E. Kümmerle and G. Heger, *J. Solid State Chem.*, 1999, **147**, 485–500.

14 W. C. Chueh, C. Falter, M. Abbott, D. Scipio, P. Furler, S. M. Haile and A. Steinfeld, *Science*, 2010, **330**, 1797–1801.

15 P. Furler, J. R. Scheffe and A. Steinfeld, *Energy Environ. Sci.*, 2012, **5**, 6098–6103.

16 W. C. Chueh and S. M. Haile, *Philos. Trans. R. Doc. London, Ser. A*, 2010, **368**, 3269–3294.

17 I. Ermanoski, J. E. Miller and M. D. Allendorf, *Phys. Chem. Chem. Phys.*, 2014, **16**, 8418–8427.

18 B. Bulfin, F. Call, M. Lange, O. LuĬĹbben, C. Sattler, R. Pitz-Paal and I. V. Shvets, *Energy Fuels*, 2015, **29**, 1001–1009.

19 B. Bulfin, B. Murphy, O. Lubben, S. Krasnikov and I. Shvets, *Int. J. Hydrogen Energy*, 2012, **37**, 10028–10035.

20 J. Lapp, J. Davidson and W. Lipiński, *Energy*, 2012, **37**, 591–600.

21 N. P. Siegel, J. E. Miller, I. Ermanoski, R. B. Diver and E. B. Stechel, *Ind. Eng. Chem. Res.*, 2013, **52**, 3276–3286.

22 H. Kaneko, T. Miura, A. Fuse, H. Ishihara, S. Taku, H. Fukuzumi, Y. Naganuma and Y. Tamaura, *Energy Fuels*, 2007, **21**, 2287–2293.

23 N. Gokon, T. Mataga, N. Kondo and T. Kodama, *Int. J. Hydrogen Energy*, 2011, **36**, 4757–4767.

24 H. Kaneko, Y. Ishikawa, C.-i. Lee, G. Hart, W. Stein and Y. Tamaura, in *ASME 2011 5th International Conference on Energy Sustainability*, 2011, pp. 1673–1680.

25 D. Marxer, P. Furler, J. Scheffe, H. Geerlings, C. Falter, V. Batteiger, A. Sizmann and A. Steinfeld, *Energy Fuels*, 2015, **29**, 3241–3250.

26 A. le Gal and S. Abanades, *Int. J. Hydrogen Energy*, 2011, **36**, 4739–4748.

27 A. le Gal and S. Abanades, *J. Phys. Chem. C*, 2012, **116**, 13516–13523.

28 A. le Gal, S. Abanades and G. Flamant, *Energy Fuels*, 2011, **25**, 4836–4845.

29 K.-S. Kang, C.-H. Kim, C.-S. Park and J.-W. Kim, *J. Ind. Eng. Chem.*, 2007, **13**, 657–663.

30 Q.-L. Meng, C. il Lee, T. Ishihara, H. Kaneko and Y. Tamaura, *Int. J. Hydrogen Energy*, 2011, **36**, 13435–13441.

31 F. Call, M. Roeb, M. SchmuĬĹcker, C. Sattler and R. Pitz-Paal, *J. Phys. Chem. C*, 2015, **119**, 6929–6938.

32 S. Abanades, A. le Gal, A. Cordier, G. Peraudeau, G. Flamant and A. Julbe, *J. Mater. Sci.*, 2010, **45**, 4163–4173.

33 G. Zhou, P. R. Shah, T. Kim, P. Fornasiero and R. J. Gorte, *Catal. Today*, 2007, **123**, 86–93.

34 H. Kaneko, S. Taku and Y. Tamaura, *Sol. Energy*, 2011, **85**, 2321–2330.

35 Y. Hao, C.-K. Yang and S. M. Haile, *Chem. Mater.*, 2014, **26**, 6073–6082.

36 M. Takacs, J. Scheffe and A. Steinfeld, *Phys. Chem. Chem. Phys.*, 2015, **17**, 7813–7822.

37 D. Bevan and J. Kordis, *J. Inorg. Nucl. Chem.*, 1964, **26**, 1509–1523.

38 P. Campserveux, J; Gerdanian, *J. Solid State Chem.*, 1978.

39 O. T. Sørensen, *J. Solid State Chem.*, 1976, **18**, 217–233.

40 M. Kuhn, S. Bishop, J. Rupp and H. Tuller, *Acta Mater.*, 2013, **61**, 4277–4288.

41 C. Jarrett, W. Chueh, C. Yuan, Y. Kawajiri, K. H. Sandhage and A. Henry, *Sol. Energy*, 2016, **123**, 57–73.

42 H. von Storch, H. Stadler, M. Roeb and B. Hoffschmidt, *Appl. Therm. Eng.*, 2015, **87**, 297–304.

43 H. von Storch, M. Roeb, H. Stadler, C. Sattler and B. Hoffschmidt, *Appl. Therm. Eng.*, 2016, **92**, 202–209.

44 J. Lapp, J. H. Davidson and W. Lipiński, *J. Sol. Energy Eng.*, 2013, **135**, 031004.

45 R. B. Diver, J. E. Miller, N. P. Siegel and T. A. Moss, ASME 2010 4th International Conference on Energy Sustainability, 2010, pp. 97–104.

46 J. Felinks, S. Brendelberger, M. Roeb, C. Sattler and R. Pitz-Paal, *Appl. Therm. Eng.*, 2014, **73**, 1006–1013.

47 S. Brendelberger, M. Roeb, M. Lange and C. Sattler, *Sol. Energy*, 2015, **122**, 1011–1022.

48 L. B. Pankratz and R. V. Mrazek, *US Bureau of Mines Bulletin*, 1982, **672**, year.

49 I. Ermanoski, *Int. J. Hydrogen Energy*, 2014, **39**, 13114–13117.

50 M. Roeb and C. Sattler, *Science*, 2013, **341**, 470–471.

51 R. Bader, L. J. Venstrom, J. H. Davidson and W. Lipiński, *Energy Fuels*, 2013, **27**, 5533–5544.

52 J. R. Scheffe, M. Welte and A. Steinfeld, *Ind. Eng. Chem. Res.*, 2014, **53**, 2175–2182.

53 C. L. Muhich, B. W. Evanko, K. C. Weston, P. Lichty, X. Liang, J. Martinek, C. B. Musgrave and A. W. Weimer, *Science*, 2013, **341**, 540–542.

54 L. J. Venstrom, R. M. De Smith, Y. Hao, S. M. Haile and J. H. Davidson, *Energy Fuels*, 2014, **28**, 2732–2742.

55 M. Lange, M. Roeb, C. Sattler and R. Pitz-Paal, *Energy*, 2014, **67**, 298–308.